Enhanced Common-Mode Noise Rejection Method Based on Impedance Mismatching Compensation for Wireless Capsule Endoscopy Systems

Won-Jun Hwang, Ki-Yun Kim, and Hyung-Jin Choi

Common-mode noise (CMN) is an unresolved problem in wireless capsule endoscopy (WCE) systems. In a WCE system, CMN originates from various electric currents found within the human body or external interference sources and causes critical demodulation performance degradation. The differential operation, a typical method for the removal of CMN rejection, can remove CMN by subtracting two signals simultaneously received by two reception sensors attached to a human body. However, when there is impedance mismatching between the two reception sensors, the differential operation method cannot completely remove CMN. Therefore, to overcome this problem, we propose an enhanced CMN rejection method. The proposed method performs not only subtraction but also addition between two received signals. Then a CMN ratio can be estimated by sufficient accumulation of division operation outcomes between the subtraction and addition outputs during the guard period. Finally, we can reject the residual CMN by combining the subtraction and addition outputs.

Keywords: Body area network, CMN, differential signaling, impedance mismatching, WCE.

Manuscript received Nov. 14, 2014; revised Feb. 3, 2015; accepted Feb. 11, 2015.

The work was supported by the Advanced Technology Center Project (Grants No. 10035991) of Korean Ministry of Knowledge Economy.

Won-Jun Hwang (corresponding author, hms4253@gmail.com) is with Samsung Electronics Co. Ltd., Suwon, Rep. of Korea.

Ki-Yun Kim (kkim@mjc.ac.kr) is with the Department of Information and Engineering, Myongji College, Seoul, Rep. of Korea.

Hyung-Jin Choi (hjchoi1@skku.edu) is with the College of Information and Communication Engineering, Sungkyunkwan University, Suwon, Rep. of Korea.

I. Introduction

In medicine, an endoscope is an essential instrument and is one that can be used to examine the digestive tract accurately. However, it is inconvenient to use a conventional wired endoscope because of the considerable discomfort it causes to patients. In addition, this conventional instrument is limited in terms of its test coverage due to its finite length [1]. For these reasons, a wireless capsule endoscope (WCE) is a suitable substitute device for a conventional endoscope [2].

WCE systems, in general, comprise two devices. One is a capsule that contains light-emitting diodes (LEDs), a camera, a transceiver, batteries, and so on. The other is a data storage device that receives and stores digital images from an in-body capsule [3].

For image data transmission/reception between an in-body capsule and its corresponding out-of-body data storage device, near field magnetic coupling–based human body communication (HBC) is more widely used as opposed to traditional radio frequency (RF) communication. This is because a magnetic field in comparison to an RF signal is less absorbed by the human body, and the battery life of the in-body capsule is increased by comparison, as RF signal generation will consume battery power [4].

Although the radiation range of a magnetic field is relatively short with that of RF communication, it can be captured by several reception sensors attached to a person's skin (or an item of their clothing) [5]–[6].

The magnetic field signal received from an in-body capsule is influenced by the human body, which makes various

distortions on the signal. Among them, common-mode noise (CMN), which is caused unstable grounding, biological currents generated from within the human body, and electrostatic currents from outside of the human body, has a significant impact on the performance of WCE systems [7]. Typically, CMN identically influences all reception sensors; thus, it can be removed by differential operation, which is a method whereby given two received signals captured by different sensors, one is subtracted from the other [8].

In a practical environment, however, the impedances of reception sensors are different from each other, for several reasons. As analyzed in [9], the characteristics of a reception sensor's impedance are dependent upon many factors, such as the adhesion level of each reception sensor, position of the reception sensors, body tissue type, a person's age, a person's sex, a person's weight, and so on. Therefore, it is hard to normalize variations in impedance of reception sensors. It is because of such impedance mismatching between reception sensors that variations in CMN magnitude are inevitable [10]–[11]. In addition to this, there remains the issue of residual CMN after the differential operation has been applied.

In a WCE system, even a small amount of residual CMN can cause critical performance degradation in demodulation at a receiver. To overcome this problem, therefore, we propose a new method that estimates and compensates impedance mismatching for removing residual CMN.

The rest of this paper is organized as follows. Section II introduces a general system model for a HBC-based WCE system. Brief descriptions of the conventional differential operation are presented in Section III, and the proposed impedance mismatching estimation/compensation method is explained in Section IV. Numerical results and analyses are presented in Section V, and a brief conclusion is drawn in Section VI.

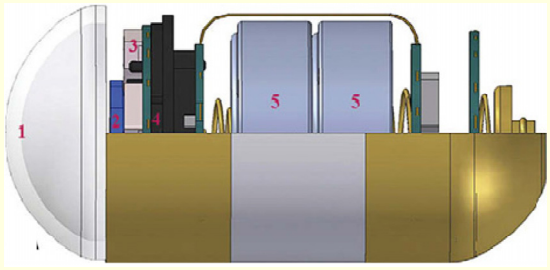

Fig. 1. HBC capsule: 1. optical dome, 2. lens, 3. LEDs, 4. image sensor, and 5. battery.

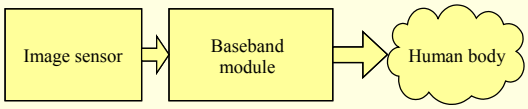

Fig. 2. Transmission process.

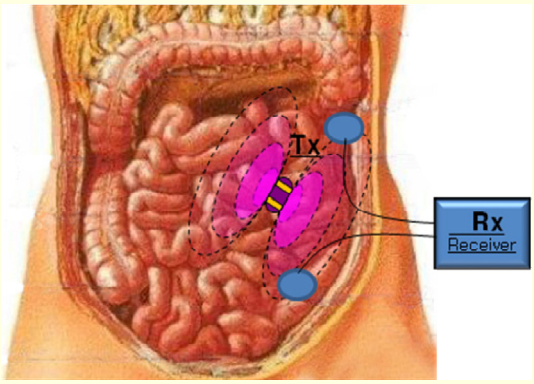

Fig. 3. Illustration of image data transmission/reception in WCE system.

II. HBC-Based WCE System Model

1. System Architecture

A. Transmitter

A WCE capsule is typically in the shape of a pill smaller than 11 mm × 22 mm. As shown in Fig. 1, basic functional components, such as LEDs, an image sensor and batteries, are embedded in the capsule. Once swallowed by a patient, the capsule will begin taking dozens of still images of the gastrointestinal tract per second, moving down from the gullet to the large intestine.

An RF module is not used in our system, so the data signal flow is simple, as shown in Fig. 2. The image data taken by the in-body capsule is modulated to baseband pulses, and then the baseband pulses are directly propagated as a low-power electric field outside of the human body through two different electrodes (+, –); that is, a low current generated from the electrodes flows through the human body as a conductor to transmit data.

B. Receiver

The transmitted image data is demodulated and recorded by a data storage device (that is, a receiver) located outside of the human body. To capture the baseband pulses, the data storage device utilizes reception sensors in the form of patches, which are attached to a patient's skin.

As shown in Fig. 3, the low-power electromagnetic signal transmitted by the in-body capsule radiates outwards (a few meters) and is simultaneously captured by the multiple patches (reception sensors) attached to the patient's skin. However, the

ETRI Journal, Volume 37, Number 3, June 2015
http://dx.doi.org/10.4218/etrij.15.0114.1322

received signal strength via each patch is variable depending on the location of the in-body capsule. To guarantee sufficient signal-to-interference-plus-noise power ratio (SINR) of the received signal, a simple receiver diversity scheme, SINR-based signal selection, is applied. Namely, the receiver chooses a few patches to demodulate the received data considering the SNR of the received signal. This patch selection process should be repeated periodically, with appropriate duration, to cope with SINR variation due to the movement of the capsule. Instead of this selection technique, other receiver diversity techniques, such as maximal ratio combining or equal gain combining [12], can also be applied; however, for the sake of simplicity, we do not consider such schemes in this paper.

2. Frame Structure

The data frame structure considered in this paper is illustrated in Fig. 4. As shown in the figure, there is a preamble period for the first 50 lines of each frame, where one line is 344 byte × 8 bit/byte × 1 symbol/bit = 2,752 symbols. The first 48 lines of preamble are used for the aforementioned patch selection process and frame synchronization. The last 2 lines of preamble are used for channel estimation/equalization. After the preamble, image data modulated by the baseband binary pulse is transmitted for the next 320 lines. Here, a periodic training sequence, called line sync, is allocated at the first 48 symbols of each data line for periodic symbol timing tracking and update of equalization filter coefficients. The guard period, during which no signal is transmitted, is a guard interval of 8 lines in length and serves to separate out each of the frames.

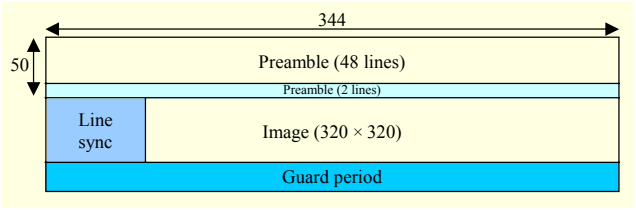

Fig. 4. Example of data frame structure for WCE system.

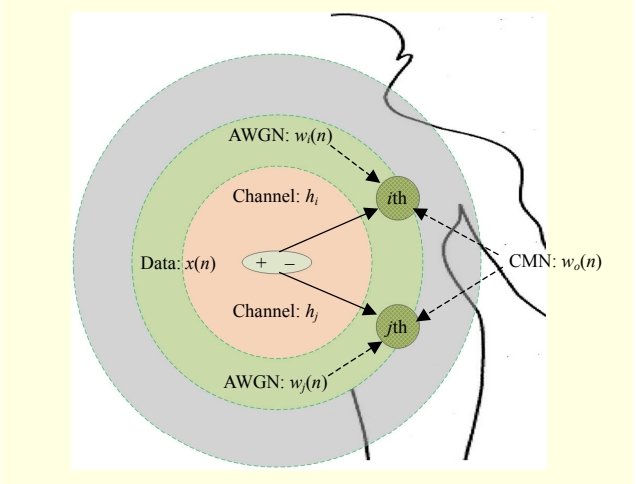

Fig. 5. Mathematical signal model.

3. Signal Model

Figure 5 shows the mathematical signal model considered in our system. When an in-body capsule transmits a data signal through the human body to patches attached to the patient (reception sensors), the resulting channel effects appear differently depending on the position of each patch. Furthermore, CMN and additive white Gaussian noise (AWGN) are added to each received signal. Now, let us model a received signal, $y_i(n)$, as follows:

$$y_i(n) = h_i \cdot x(n) + w_o(n) + w_i(n), \quad (1)$$

where h_i is the channel impulse response (CIR) of the ith patch. In this paper, we assume that h_i has a semi-static characteristic since the movement speed of the in-body capsule is sufficiently slow. Also in (1), $x(n)$ is the transmitted data signal from the in-body capsule, $w_o(n)$ is the CMN, and $w_i(n)$ is the AWGN of the ith sensor. Because the magnitude of the CMN can be significantly larger than that of the data signal, this can cause serious demodulation performance degradation.

In a similar way, the received signal via the jth patch, $y_j(n)$, can be expressed as follows:

$$y_j(n) = h_j \cdot x(n) + w_o(n) + w_j(n), \quad (2)$$

where h_j and $w_j(n)$ are the CIR of the jth patch and AWGN of the jth patch, respectively. Note that h_i and h_j are mutually independent when the ith and jth patches are sufficiently isolated from each other.

III. Conventional Solution

1. Differential Operation for CMN Rejection

As mentioned previously, the differential operation is generally considered for removing CMN. Figure 6 shows the conceptual circuit structure of the differential operation. To perform the differential operation, we select a pair of received signals $y_i(n)$ and $y_j(n)$ among N_{patch} candidate signals. Then, the differential operation output, $y_{i,j}(n)$, is obtained by subtraction between the two selected received signals as follows:

$$y_{i,j}(n) = y_i(n) - y_j(n) = (h_i - h_j)x(n) + w_i(n) - w_j(n), \quad (3)$$

where $1 \le i \le N_{\text{patch}}$, $1 \le j \le N_{\text{patch}}$, and $i \ne j$. As shown in (3), the

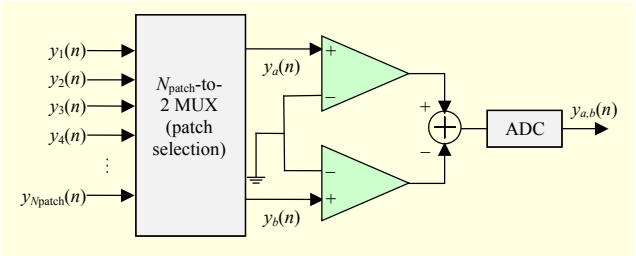

Fig. 6. Block diagram of conventional differential operation.

CMN in each received signal has the same phase; thus, CMN can be removed by a subtraction operation. Meanwhile, the data signals received from another patch have a different phase due to the independent channel effect in each patch sensor; hence, they are not fully removed by the subtraction. With N_{patch} candidate signals, there are $N_{\text{patch}}C_2$ ways to make a pair of patches. Among them, we choose the *best* (maximum received signal power) pair of patch indices, a and b, such that the following condition is met:

$$(a,b) = \arg\max_{(i,j)} \left\{ \mathrm{E}\left[\left(y_i(n) - y_j(n) \right)^2 \right] \right\}. \quad (4)$$

The expectation operation in (4) should be done for every patch combination case. These massive signal averaging operations can be simultaneously done by parallel circuits, but this approach obviously increases the hardware complexity of a receiver. Thus, in our system, the operations are sequentially performed during the preamble period. This alternative approach requires a large preamble size, since we generally suppose that at least 4,000 to 5,000 symbols will be accumulated for each combination case for sufficient noise reduction. This is the reason why the system uses as many as 48 lines (= 132,096 symbols) of preamble for patch selection.

The finally selected differential operation output signal, $y_{a,b}(n)$, can be written as

$$y_{a,b}(n) = (h_a - h_b)x(n) + w_a(n) - w_b(n). \quad (5)$$

After the above differential operation and patch selection, $y_{a,b}(n)$ is converted to digital samples by an analog-to-digital converter (ADC). After that, the channel coefficient, $(h_i - h_j)$, is estimated and compensated by a channel estimator/equalizer, and then data signal $x(n)$ can be demodulated.

2. Problem of Conventional Method

In a practical environment, the impedance of each patch sensor is variable due to both the patch's adhesion and the position of the patch; thus, the impedance values of any two randomly selected patch sensors can be different from each other. In consideration of patch impedance, $y_a(n)$, $y_b(n)$, and $y_{a,b}(n)$ are written as follows:

$$y_a(n) = h_a R_a \cdot x(n) + R_a \cdot w_o(n) + w_a(n), \quad (6)$$

$$y_b(n) = h_b R_b \cdot x(n) + R_b \cdot w_o(n) + w_b(n), \quad (7)$$

$$y_{a,b}(n) = (h_a R_a - h_b R_b)x(n) + (R_a - R_b)w_o(n) + w_a(n) - w_b(n), \quad (8)$$

where R_a and R_b are the impedance gains of the ath and bth patches, respectively. These values depend on the adhesion levels of the corresponding patches. As shown in (8), there remains residual CMN after the differential operation due to impedance mismatching, and the amount of residual CMN is proportional to a difference between the two impedance gains; that is, $R_a - R_b$. Obviously, when the residual CMN still remains, the quality of the received signal can be degraded seriously.

IV. Proposed Solution

In this section, we propose an enhanced differential operation method that can overcome the impedance mismatching problem described in the previous section. The proposed method consists of two operational steps — CMN ratio estimation and residual CMN rejection by weighted combining. The proposed method performs not only the differential operation but also a summation operation between the two received signals. Then, the CMN ratio can be estimated by sufficient accumulation of division operation outcomes between the subtraction output and the addition output during a guard period. Finally, we can reject any residual CMN by combining the two outputs considering the estimated CMN ratio.

Figure 7 shows the conceptual circuit structure of the proposed method, and the full procedure of the proposed method shown in the figure is described as follows.

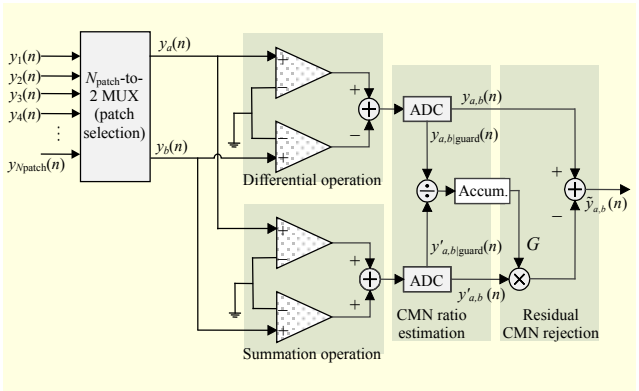

Fig. 7. Block diagram of proposed solution.

ETRI Journal, Volume 37, Number 3, June 2015
http://dx.doi.org/10.4218/etrij.15.0114.1322

1. CMN Ratio Estimation

Considering the fact that no data is transmitted during a guard period, we can use a guard period signal to estimate the impedance ratio without interference from the data signal. The differential operation output via two selected patches (ath patch and bth patch) in the guard period $y_{a,b|\text{guard}}(n)$ can be expressed as follows:

$$y_{a,b|\text{guard}}(n) = (R_a - R_b)w_o(n) + w_a(n) - w_b(n). \quad (9)$$

Also, the summation operation outputs via the two patches in the data period and the guard period, $y'_{a,b}(n)$ and $y'_{a,b|\text{guard}}(n)$, are given by

$$y'_{a,b}(n) = (h_a R_a + h_b R_b)x(n) + (R_a + R_b)w_o(n) + w_a(n) + w_b(n), \quad (10)$$

$$y'_{a,b|\text{guard}}(n) = (R_a + R_b)w_o(n) + w_a(n) + w_b(n). \quad (11)$$

By comparing (9) with (11), we can see that the ratio between the residual CMN in the differential operation output and that in the summation operation output is $(R_a-R_b)/(R_a+R_b)$. This CMN ratio value can be obtained by the accumulation of division operation outcomes between $y_{a,b|\text{guard}}(n)$ and $y'_{a,b|\text{guard}}(n)$. As mentioned in Section II-2, the guard period in our system model is 8 lines (= 2,752 × 8 = 22,016 symbols) in length per frame, and N_{sum} symbols of them can be used for accumulation. Then, the estimated CMN ratio G is given by

$$G = \frac{1}{N_{\text{sum}}}\sum_n \frac{y_{a,b|\text{guard}}(n)}{y'_{a,b|\text{guard}}(n)} = \frac{1}{N_{\text{sum}}}\sum_n \frac{(R_a-R_b)w_o(n)+w_a(n)-w_b(n)}{(R_a+R_b)w_o(n)+w_a(n)-w_b(n)} \approx \frac{(R_i-R_j)}{(R_i+R_j)}. \quad (12)$$

2. Residual CMN Rejection

The estimated G can be used as a weighting value to combine $y_{a,b}(n)$ with $y'_{a,b}(n)$. Then, the output of the weighted summation $\tilde{y}_{a,b}(n)$ can be expressed as

$$\begin{aligned}\tilde{y}_{a,b}(n) &= y_{a,b}(n) - Gy'_{a,b}(n)\\ &= \{R_a h_a - R_b h_b - G(R_a h_a + R_b h_b)\}x(n)\\ &\quad + (R_a - R_b)w_o(n) - G(R_a + R_b)w_o(n)\\ &\quad + w_a(n) - w_b(n) - G\left(w_a(n) + w_b(n)\right)\\ &\approx \left\{R_a h_a - R_b h_b - \frac{R_i - R_j}{R_i + R_j}(R_a h_a + R_b h_b)\right\}x(n)\\ &\quad + w_a(n) - w_b(n) - \frac{R_i - R_j}{R_i + R_j}\left(w_a(n) + w_b(n)\right).\end{aligned} \quad (13)$$

As shown in (13), the residual CMN can be perfectly rejected when the weight value G is ideally estimated. Since the estimation accuracy of G is fairly high with sufficient accumulation, the proposed method can remove nearly all residual CMN components, even in a practical environment.

V. Simulation and Analysis

In this section, we present various simulation results and numerical analysis that compares the proposed CMN rejection method with the conventional method in terms of signal-to-CMN-plus-noise power ratio (SCNR) distribution and bit error rate (BER) performance. Major simulation parameters are shown in Table 1.

As mentioned previously, the impedance gains R_a and R_b are random variables depending on the adhesion level between the corresponding patch and skin. The distribution of such impedance gains has not yet been studied; thus, in this paper, we simply assume that R_a and R_b are independent random variables with Gaussian distribution and mean and variance of 1 and σ_p^2 (= 0.1 or 0.01), respectively.

1. SCNR Distribution Evaluation

From (8), the SCNR of the conventional method can be derived as follows, where σ_I^2 and σ_N^2 denote the signal-to-CMN power ratio (SCR) and SNR, respectively:

Table 1. Simulation parameters.

Parameter	Value
Carrier frequency	Baseband
System bandwidth	10 MHz
Modulation	NRZ (Non-Return-to-Zero)
Channel model	Rician (K = 8) and Rayleigh single-path fading
Patch impedance mean	1
Patch impedance variance (σ_p^2)	0.01–0.1
Signal-to-CMN power ratio (σ_I^2)	–10 dB –10 dB
SNR measurement for patch selection	Ideal
Channel estimation	Ideal
# of patches (N_{patch})	8
# of accumulated symbols for CMN ratio estimation (N_{sum})	2,752 symbols (1 line)

$$\mathrm{SCNR}_{y_{a,b}} = \mathrm{E}\left[\frac{\begin{bmatrix}\{(R_a h_a - R_b h_b)x(n)\} \\ \times\{(R_a h_a - R_b h_b)x(n)\}^*\end{bmatrix}}{\begin{bmatrix}\{(R_a - R_b)w_o(n) + w_a(n) - w_b(n)\} \\ \times\{(R_a - R_b)w_o(n) + w_a(n) - w_b(n)\}^*\end{bmatrix}}\right]$$

$$= \frac{\left[R_a^2 \overbrace{\mathrm{E}\left[h_a \times h_a^*\right]}^{=1} + R_j^2 \overbrace{\mathrm{E}\left[h_b \times h_b^*\right]}^{=1}\right] \times \overbrace{\mathrm{E}\left[x(n) \times x^*(n)\right]}^{=1}}{\begin{bmatrix}(R_a - R_b)^2 \underbrace{\mathrm{E}\left[w_o(n) \times w_o^*(n)\right]}_{=\sigma_I^2} \\ + \underbrace{\mathrm{E}\left[w_a(n) \times w_a^*(n)\right]}_{=\sigma_N^2} + \underbrace{\mathrm{E}\left[w_b(n) \times w_b^*(n)\right]}_{=\sigma_N^2}\end{bmatrix}} \quad (14)$$

$$= \frac{(R_a^2 + R_b^2)}{(R_a - R_b)^2 \sigma_I^2 + 2\sigma_N^2}.$$

From (14), we can see that the SCNR of the conventional method will decrease when R_a and R_b are highly mismatched.

In the same way, the SCNR of the proposed method can be derived from (13) as follows, assuming that the weight value G is ideally estimated:

$$\mathrm{SCNR}_{\tilde{y}_{a,b}}$$

$$= \mathrm{E}\left[\frac{\begin{bmatrix}\left[\left\{R_a h_a - R_b h_b - \frac{R_i - R_j}{R_i + R_j}(R_a h_a + R_b h_b)\right\}x(n)\right] \\ \times\left[\left\{R_a h_a - R_b h_b - \frac{R_i - R_j}{R_i + R_j}(R_a h_a + R_b h_b)\right\}x(n)\right]^*\end{bmatrix}}{\begin{bmatrix}\left\{w_a(n) - w_b(n) - \frac{R_i - R_j}{R_i + R_j}\left(w_a(n) + w_b(n)\right)\right\} \\ \times\left\{w_a(n) - w_b(n) - \frac{R_i - R_j}{R_i + R_j}\left(w_a(n) + w_b(n)\right)\right\}^*\end{bmatrix}}\right]$$

$$= \frac{R_a^2\left(1 - \frac{R_a - R_b}{R_a + R_b}\right)^2 + R_b^2\left(1 + \frac{R_a - R_b}{R_a + R_b}\right)^2}{2\left[1 + \left(\frac{R_a - R_b}{R_a + R_b}\right)^2\right]\sigma_N^2}. \quad (15)$$

It is obvious that the SCNR of the proposed method will be equal to that of the conventional method when there is no impedance mismatching ($R_a = R_b$). Meanwhile, (15) cannot be simply compared with (14) when impedance mismatching occurs ($R_a \neq R_b$), since not only the noise power but also the signal power in (15) depends on the CMN ratio. Thus, in this subsection, we evaluate the two methods in terms of SCNR distribution obtained by numerical simulation.

Figures 8 to 10 illustrate the SCNR comparisons for various SCR values (from –10 dB to 10 dB) and a fixed SNR value (10 dB). From these figures, we can confirm that the proposed method provides relatively large SCNR gain in low-SCR

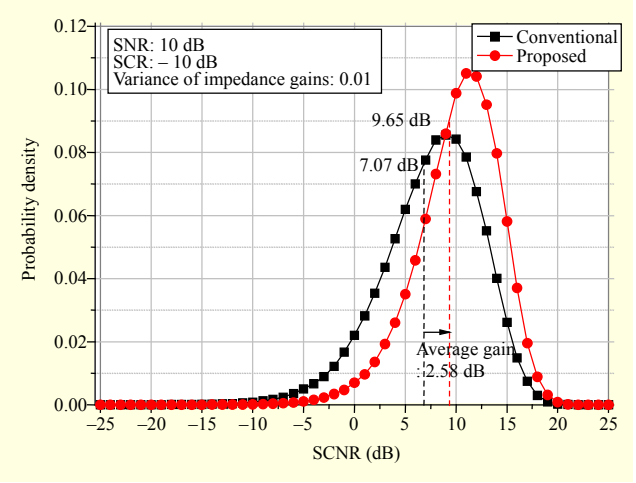

Fig. 8. SCNR distribution comparison (SCR = –10 dB).

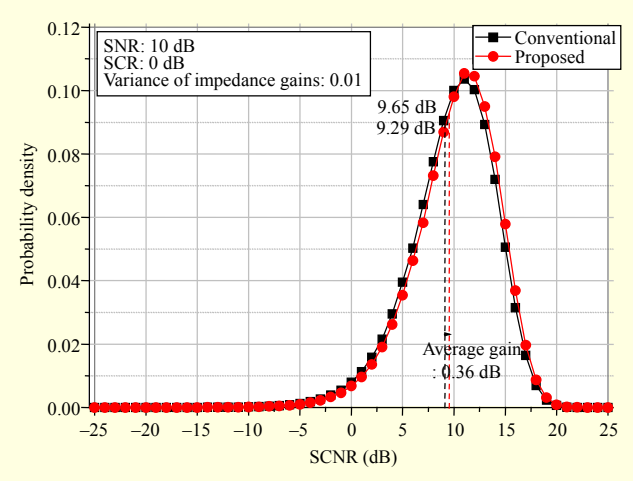

Fig. 9. SCNR distribution comparison (SCR = 0 dB).

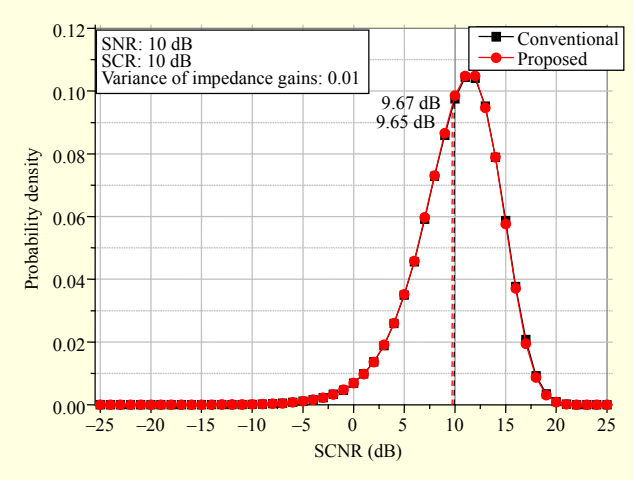

Fig. 10. SCNR distribution comparison (SCR = 10 dB).

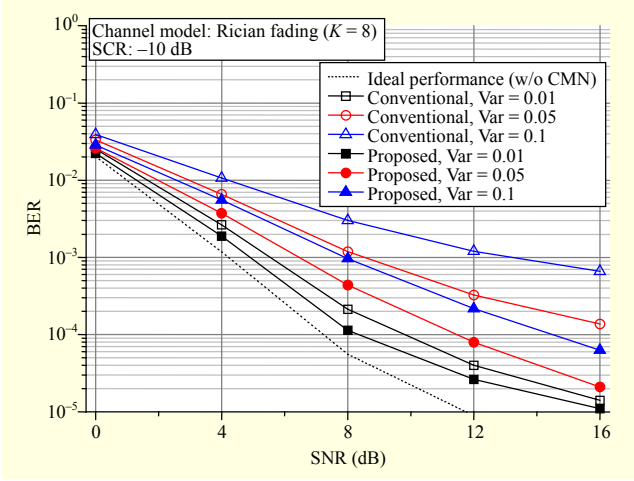

Fig. 11. BER comparisons (Rician fading channel, SCR = –10 dB).

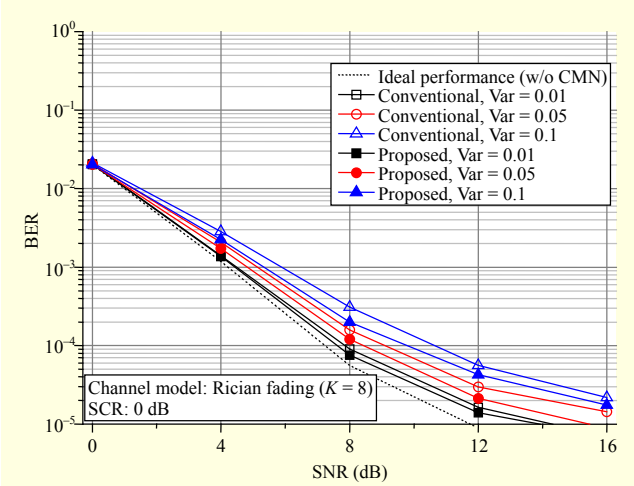

Fig. 12. BER comparisons (Rician fading channel, SCR = 0 dB).

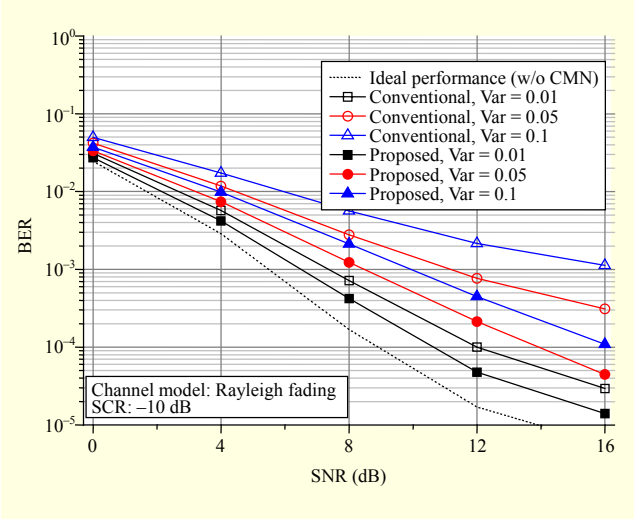

Fig. 13. BER comparisons (Rayleigh fading channel, SCR = –10 dB).

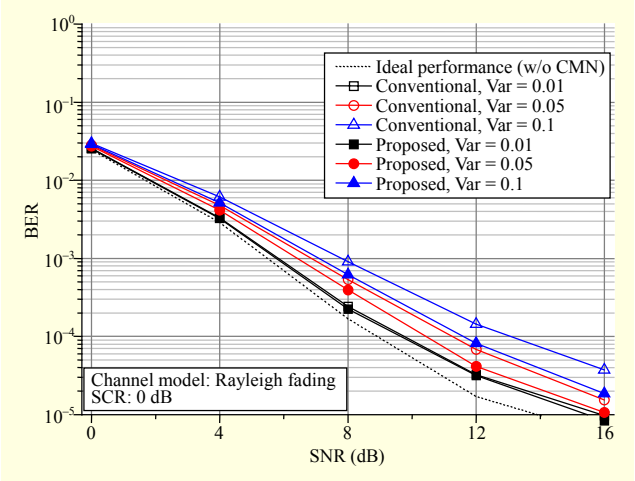

Fig. 14. BER comparisons (Rayleigh fading channel, SCR = 0 dB).

environments. As shown in Fig. 8, we can obtain an SCNR gain of approximately 2.58 dB when SCR = –10 dB. Moreover, the SCNR distribution of the proposed method does not depend on the SCR, which is in contrast to the conventional method; thus, the proposed method provides a stable demodulation performance in the case of impedance mismatching.

Unfortunately, the performance gain is reduced to 0.36 dB when SCR = 0 dB. Even when SCR is equal to or greater than 10 dB, some SCNR loss occurs. However, this performance loss is negligible, smaller than 0.1 dB. Moreover, in consideration of a practical environment for WCE, SCR is generally lower than 10 dB, since the transmit power of an in-body capsule is extremely limited so as to guarantee a sufficient operation time and avoid damage to the body [13]. From these results, therefore, we can confirm that the proposed method provides considerable SCNR gain in a practical operation environment for WCE.

2. BER Evaluation

In this subsection, we present a comparison of BER performance between the conventional method and the proposed CMN rejection method considering two typical fading channel models — Rician fading channel (K = 8) and Rayleigh fading channel.

Figures 11 to 14 illustrate the BER performance comparisons. As shown in the figures, the proposed method has a better BER performance compared to the conventional method in all cases where the variances of patch impedances are between 0.01 and 0.1. Specifically, the conventional method shows a serious performance degradation when the patch impedance variance is large and SCR is low, since the residual CMN increases under these conditions. On the other

hand, the proposed method is less affected by the patch impedance variance. From the figures, consequentially, we can see that the BER performance gain of the proposed method increases even in worse conditions. Obviously, this result means that the proposed method enables a WCE receiver to perform stably in a practical operation environment.

VI. Conclusion

This paper proposed a new method to estimate and compensate impedance mismatching for removing residual CMN in a HBC-based WCE system. The proposed method performs additional summation operations with a traditional differential operation method. The two operation outcomes are used not only to estimate CMN ratio but also to create the CMN-removed received signal through a weighted combining scheme. Extensive simulation results and mathematical analysis verified that the proposed method provided SCNR gain, which led to a remarkable enhancement in the demodulation performance of the WCE receiver used in the simulations.

References

[1] B. Chi et al., "A 2.4 GHz Low-Power Wireless Transceiver Analog Front-End for Endoscopy Capsule System," *IEEE Int. Symp. Circuits Syst.*, Island of Kos, Greece, May 21–24, 2006, pp. 4907–4910.

[2] G. Iddan et al., "Wireless Capsule Endoscopy," *Nature*, vol. 405, May 2000, pp. 417–418.

[3] S.H. Lee et al., "A Wideband Spiral Antenna for Ingestible Capsule Endoscope Systems: Experimental Results in a Human Phantom and a Pig," *IEEE Trans. Biomed. Eng.*, vol. 58, no. 6, June 2011, pp. 1734–1741.

[4] K.-Y. Kim et al., "A Comparison of Communication Techniques for Capsule Endoscopes," *IEEE APCC*, Sabah, Malaysia, Oct. 2–5, 2011, pp. 761–764.

[5] K. Nagata and Y. Kado, "Analysis of Transmission Quality in Technology for In-Body to Off-Body MHz Band near Field Coupling Communication," *EuCAP*, Gothenburg, Sweden, Apr. 8–12, 2013, pp. 789–793.

[6] M. Ahmadian et al., "Data Transmission for Implantable Microsystems Using Magnetic Coupling," *IEE Commun.*, Apr. 2005, pp. 247–250.

[7] K. Kim et al., "A Design of a High-Speed and High-Efficiency Capsule Endoscopy System," *IEEE Trans. Biomed. Eng.*, vol. 59, no. 4, Apr. 2012, pp. 1005–1011.

[8] R. Nagai et al., "Near-Field Coupling Communication Technology for Human-Area Networking," *Systemics, Cybern. Informat.*, vol. 10, no. 6, 2012, pp. 14–18.

[9] N. Vidal et al., "Detuning Study of Implantable Antennas Inside the Human Body," *Electromagn. Res.*, vol. 124, 2012, pp. 265–283.

[10] M. Shinagawa et al., "Noise Analysis for Intra-body Communication Based on Parasitic Capacitance Measurement," *Meas.*, vol. 51, May 2014, pp. 206–213.

[11] A. Sasaki et al., "Signal-to-Noise Ratio Analysis of a Noisy-Channel Model for a Capacitively Coupled Personal Area Network," *IEEE Trans. Antennas Propag.*, vol. 61, no. 1, Sept. 2012, pp. 390–402.

[12] M.K. Simon and M.-S. Alouini, "*Digital Communication over Fading Channels: A Unified Approach to Performance Analysis*," 2nd ed., New York, NY, USA: Wiley, 2005.

[13] M. Sendoh, K. Ishiyama, and K.-I. Arai, "Fabrication of Magnetic Actuator for Use in a Capsule Endoscope," *IEEE Trans. Magn.*, vol. 39, no. 5, Sept. 2003, pp. 3232–3234.

Won-Jun Hwang received his BS and MS degrees in electrical engineering from the School of Electrical and Computer Engineering, Sungkyunkwan University, Suwon, Rep. of Korea, in 2009 and 2011, respectively and his PhD degree in electrical engineering from the Department of IT Convergence, Sungkyunkwan University, in 2015. Since 2015, he has been an engineer with Samsung Electronics Co. Ltd., Suwon, Rep. of Korea. His main research interests are mobile communication system engineering; channel estimation; interference mitigation; adaptive modulation and coding; OFDM; MIMO; and signal processing for synchronization.

Ki-Yun Kim received his BS, MS, and PhD degrees in electrical engineering from the College of Electrical and Computer Engineering, Sungkyunkwan University, Suwon, Rep. of Korea, in 1997, 1999, and 2002, respectively. From 2001 to 2008, he worked for Samsung Thales, Kihueng, Rep. of Korea, as a senior engineer. From 2006 to 2007, he was a postdoctoral fellow with the Department of Electrical Engineering, University of California, Los Angeles, CA, USA. Since 2008, he has been a faculty member with the Department of Electrical Engineering, Myongji College, Seoul, Rep. of Korea and currently holds the rank of associate professor. His main research interests are digital communication systems (mobile, satellite, and military), biomedical engineering, and signal processing.

Hyung-Jin Choi received his BS degree in electronic engineering from the College of Engineering, Seoul National University, Rep. of Korea, in 1974; his MS degree in electrical and electronics engineering from the Korea Advanced Institute of Science and Technology, Daejeon, Rep. of Korea, in 1976; and his PhD degree in electrical engineering (communications major) from the College of Engineering, University of Southern California, Los Angeles, USA, in 1982. From 1976 to 1979, he worked for the Central Research Lab. of the Gold Star Co., Seoul, Rep. of Korea, as a research engineer. From 1983 to 1989, he worked for Lincom Corp., Los Angeles, CA, USA. Since 1989, he has been a faculty member with the Department of Electronics Engineering (now, the School of Information and Communication Engineering), Sungkyunkwan University, Suwon, Rep. of Korea, where he currently holds the rank of professor. His main research interests are mobile radio engineering; satellite communications; communication system engineering; and digital modulation/demodulation with associated signal processing and synchronization.